ISSN 0016-8521, Geotectonics, 2016, Vol. 50, No. 3, pp. 223–237. © Pleiades Publishing, Inc., 2016.
Original Russian Text © S.Yu. Sokolov, Yu.A. Zaraiskaya, A.O. Mazarovich, V.N. Efimov, N.S. Sokolov, 2016, published in Geotektonika, 2016, No. 3, pp. 3–18.

Spatial Instability of the Rift in the St. Paul Multifault Transform Fracture System, Atlantic Ocean

S. Yu. Sokolov[a], Yu. A. Zaraiskaya[a], A. O. Mazarovich[a], V. N. Efimov[a], and N. S. Sokolov[b]

[a] *Geological Institute, Russian Academy of Sciences, Pyzhevskii per. 7, Moscow, 119017 Russia*

[b] *Severo-Zapad, Pervyi Dorozhnyi pr. 9, Moscow, 117545 Russia*

e-mail: sysokolov@yandex.ru

Received September 7, 2015

Abstract—The structure of the acoustic basement of the eastern part of the St. Paul multifault transform fracture system hosts rift paleovalleys and a paleonodal depression that mismatch the position of the currently active zones. This displacement zone, which is composed of five fault troughs, is unstable in terms of the position of the rift segments, which jumped according to redistribution of stresses. The St. Paul system is characterized by straightening of the transform transition between two remote segments of the Mid-Atlantic Ridge (MAR). The eastern part of the system contains anomalous bright-spot-like reflectors on the flattened basement, which is a result of atypical magmatism, which forms the standard ridge relief of the acoustic basement. Deformations of the acoustic basement have a presedimentation character. The present-day deformations with lower amplitude in comparison to the basement are accompanied by acoustic brightening of the sedimentary sequence. The axial Bouguer anomalies in the east of the system continue to the north for 120 km from the active segments of the St. Paul system. Currently seismically active segments of the spreading system are characterized by increasing amplitudes of the E–W displacement along the fault troughs. Cross-correlation of the lengths of the active structural elements of the MAR zone (segments of the ridge and transform fracture zones of displacement) indicates that, statistically, the multifault transform fracture system is a specific type of oceanic strike-slip faults.

Keywords: transform fracture zone, multifault system, deformation of sedimentary cover, seismic section, St. Paul

DOI: 10.1134/S0016852116030110

INTRODUCTION

The tectonogenesis in the Mid-Atlantic Ridge (MAR) zone forms a system of two major structural elements: a rift zone and transform fracture zones. As a rule they are orthogonal to each other, seismically active, and, according to numerous data including earthquake foci, are formed by extension and displacement processes. The tectonogenesis of the longitudinal MAR segments is accompanied by various events of the unstable position of the spreading system center: rift jumps, rift overlaps, nontransform displacement, along-the-axis displacement [1], and others. Tectonogenesis along the transform fracture zones may be accompanied by complex deformations [9] related to transpression or transtension (or their combination), as well as a change in direction of vectors and rates of plate movements divided by the break. The multifault transform fracture system [4], which is composed of three and more fault troughs with almost equal small distance, results in additional instability: the migration of segments of the rift zone within the narrow interfault space of the multifault system.

The multifault systems are series of near-parallel, closely located trenches of transform fracture zones with a total width of the few hundred miles. They form areas of the oceanic floor with complex morphology of at least two classes. The first class is characterized by numerous transverse and median ridges (Arkhangel'skii–Doldrums–Vernadskii–Bogdanov) in contrast to the second class (St. Paul). These complexes are considered a specific type of plate boundaries (multifault transform fracture plate boundary) [16]. Multifault systems (the fault zones Siqueiros in the Pacific Ocean [14], Andrew Bain in the Indian Ocean [21], St. Paul in the Atlantic Ocean [11]) could host superimposed spreading centers [14] with a specific magmatism (the Garrett Fracture Zone in the southern part of the Pacific Ocean [24]). This work focuses on the second class of the systems with the St. Paul system as an example.

In the Atlantic Ocean, there are several multifault and double transform fracture systems (St. Paul, Romanche, Arkhangel'skii– Doldrums–Vernadskii–Bogdanov, Charlie–Gibbs, etc.) and most of them are confined to areas of maximum latitudinal displace-

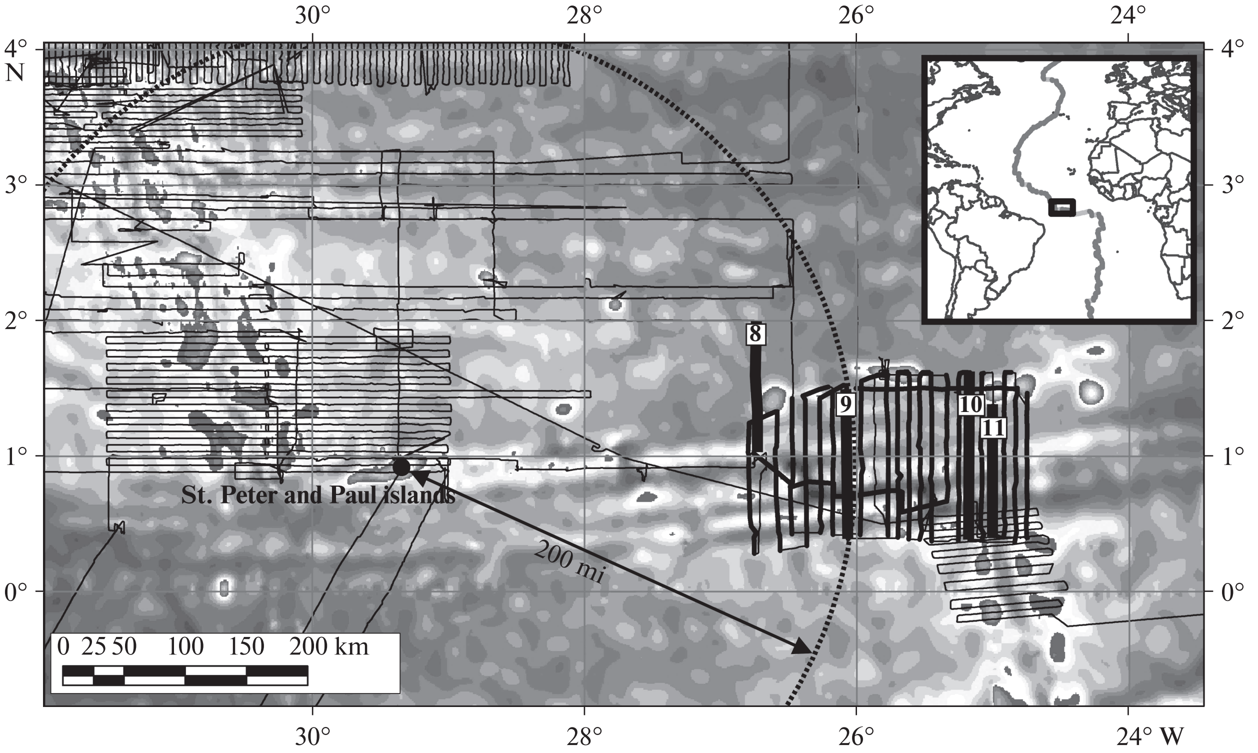

Fig. 1. Area of St. Paul multifault transform fracture system and work scheme of seventh cruise of R/V *Akademik Nikolai Strakhov* (GIN RAS, 1988). Inset map, position of area studied in Atlantic relative to MAR. Bold lines, survey area in eastern part of St. Paul fracture system; dotted circle, 200-mile economic zone of Brazil around St. Peter and Paul islands. Isobath of interception of volcanic seamounts and highlands of ridge is 2500 m. Numbers in squares indicate position of seismic sections in Figs. 8–11.

ment of the MAR's main zone in the equatorial region (Fig. 1, inset map) and to manifestations of the cold upper mantle, according to the seismographic data [8]. The boundaries of the cold zones in the upper mantle coincide with the main segmentation of the ocean in terms of the age of the onset of spreading after breakup of the supercontinent. The St. Paul multifault system (Fig. 1) is the most striking example of this event, and its eastern part has been studied by areal geophysical survey from on board the R/V *Akademik Nikolai Strakhov* on the seventh cruise of the Geological Institute, Russian Academy of Sciences (GIN RAS), led by G.B. Udintsev [5]. The aim of this work is to describe the instability of the multifault zone using multibeam bathymetry, seismicity, sedimentary cover distribution, Bouguer gravitational anomalies, and bottom sampling.

STATISTICAL CHARACTERISTICS OF MAR STRUCTURAL ELEMENTS

The MAR segments and areas of displacement of transform fracture zones were digitized in the 18th version of an altimetry grid [20]. The rift segments and offset transform fracture zones are active MAR structural elements, and their spatial distribution and frequency of occurrence are the major characteristics included in the common MAR segmentation. The latter is based on certain variable geological–geophysical characteristics: the age of the onset of spreading and geochemical anomalies of the igneous rocks [2]. The largest segments in these schemes are divided by especially extended transform fracture zones. Segmentation along the MAR similar in geometry is traced by seismotomography of the upper mantle [8]. Hierarchy (the principle which combines MAR segments in larger chains) is a significant feature of all schemes. The structural features (sizes of MAR segments or offset zones) or along-axis variations in geophysical parameters [1] are generally dominant, despite the fact that zero level domains are substantiated by other parameters. Thus, the construction of a hierarchy is a complex multifactor task, which is beyond the scope of our work. The study of the local instability uses common statistical characteristics of the primary active elements rather than combination methods and omits the problems of hierarchy.

Figure 2 shows the distribution of MAR segments less than 230 km long by intervals of 5 km. MAR nontransform displacements as the boundaries of segments were not considered. We analyzed only transform fracture zones with clearly expressed displacement zones. The major frequencies of the MAR fragmentation with some generalization include three

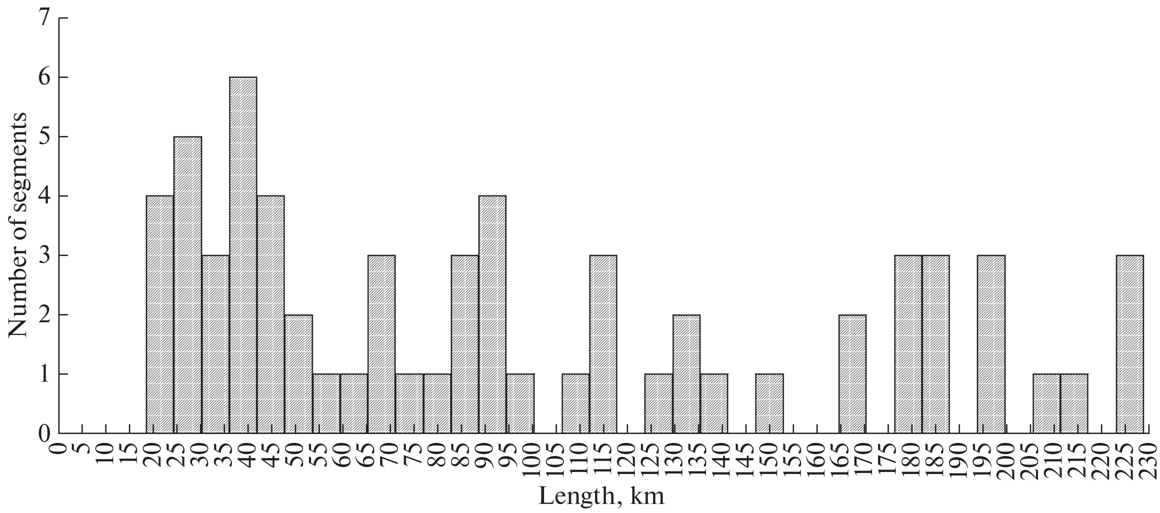

Fig. 2. Distribution of number of MAR segments less than 230 km in lengths and ranges of 5 km. Here and in Fig. 3, all longer segments are characterized by frequency of occurrence of 1 in estimated range.

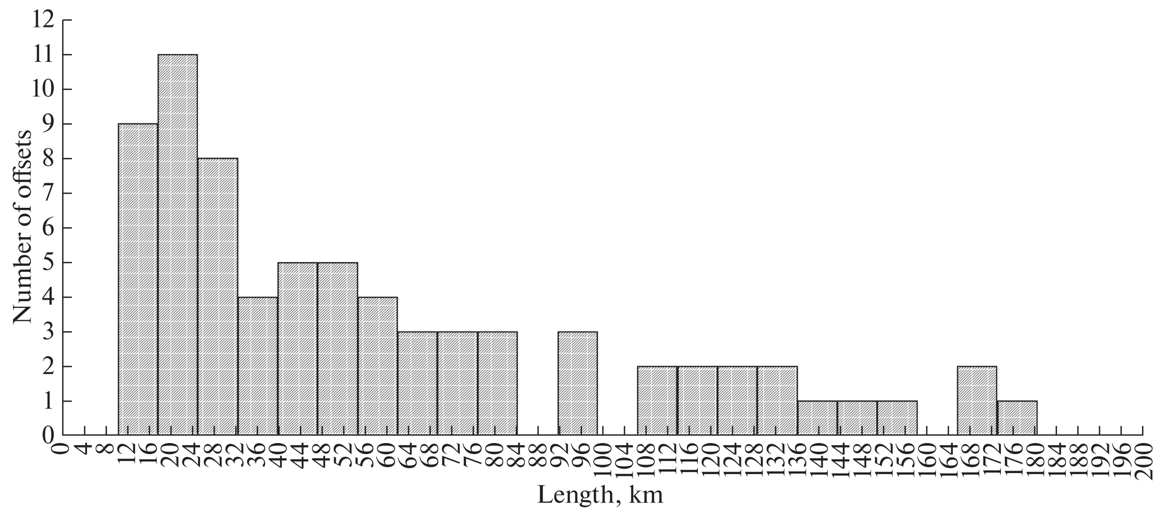

Fig. 3. Distribution of number of offset zones of transform fracture zones with lengths of <200 km with ranges of 7 km.

groups in the ranges of 20–55, 55–160, and 160–300 km. Twelve of 83 MAR segments of larger size (>300 km long) make up 7920 (~50%) of the total MAR length of 16 100 km. The largest of them, in the absence of offset zones and the presence of nontransform displacements inside, correspond to MAR areas with plume seismotomographic anomalies in the mantle (Iceland, Azores, Ascension, Gough-Tristan da Cunha). Thus, the interpretation of their origin has a clear physical meaning: plume zones are less viscous and often host (or do not host) nontransform displacements and rare transform fracture zones. Two groups with average ranges of 25 and 40 km occur inside the very first, most numerous range. Similar values of pseudoperiodical fragmentation along the axial zone are also abundant in the northern part of the Indian Ridge and the Southwest Indian Ridge.

The distribution of offset zones (Fig. 3) is asymmetric (as well as the distribution of MAR segments) without expressed polymodality, although there are features of additional maximums. The value of the major maximum of occurrence is ~22 km, which that is close to those of the major maximums of occurrence of MAR segments (25 km). The maximum fragmentation along the extension zones coincides with those along the displacement zones.

Figure 4 shows the cross-correlation of extended MAR segments and offset zones of transform fracture zones. The indicated parameters were compared for the transform fracture zones and segments north of

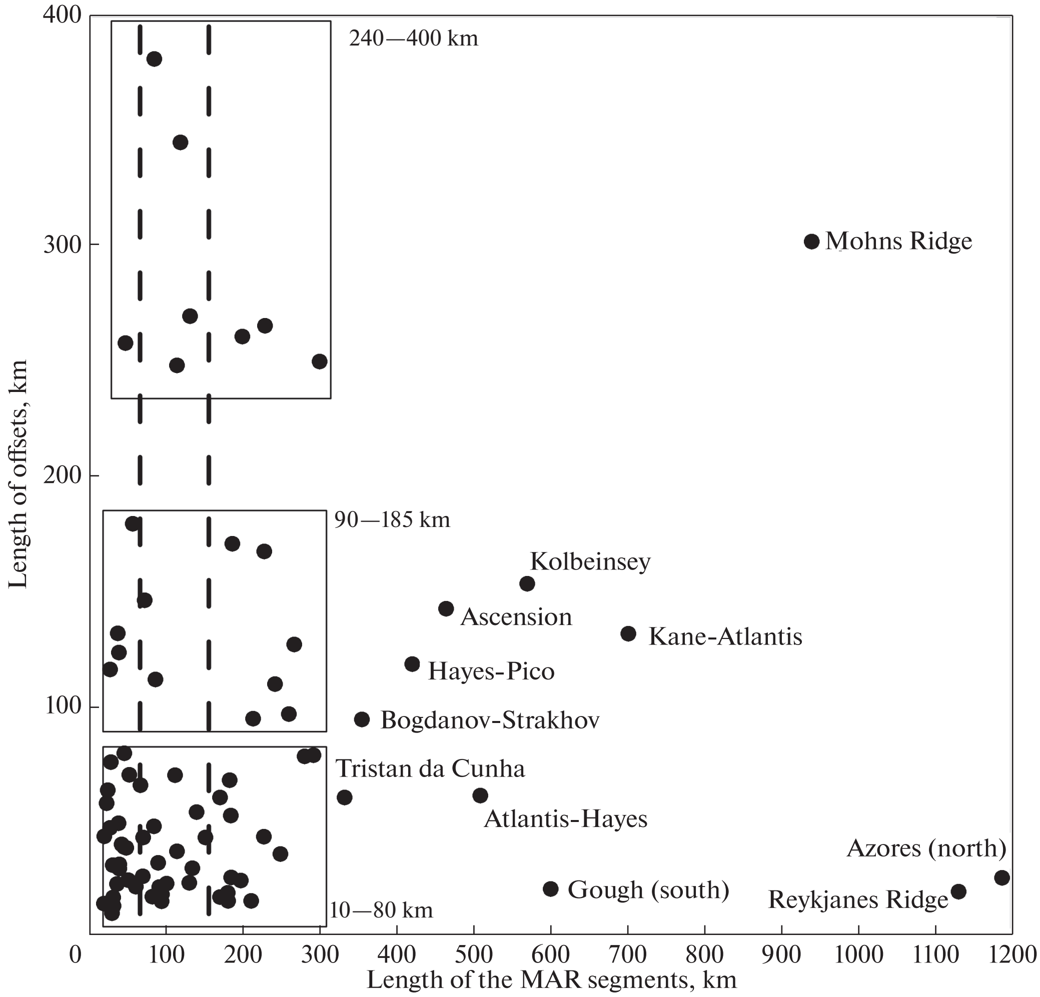

Fig. 4. Cross-correlation of length of MAR segments and length of offset zones of transform fracture zones. Frames, spatial groups by offset lengths; dotted lines, groups of lengths of MAR segments. Elements with longer (>300 km) MAR segments are named.

them. The figure lacks the Romanche Transform Fracture Zone with a displacement of ~750 km, which is unique and falls outside the major values. The dotted lines divide three groups of lengths of MAR segments in the above ranges. Elements with long (>300 km) MAR segments have been named: all of them are unique and coincide with "hot" seismotomographic anomalies (Fig. 5), which is evident from the position of the centers of MAR segments of large length.

First of all, we should note the two-dimensional segmentation of the point cloud in the cross-correlation (Fig. 4) of three groups for both parameters. Along the MAR axis within the first group, the extensions of displacements are compact and coincide with one-dimensional MAR segments (Fig. 2). Toward the offset lengths, one can see three groups of ranges with comparable sizes but with large empty range between the second and third groups (from 185 to 240 km). A similar geometry of the fragmentation frequencies of the extension and shift structures may indicate a similar average (in terms of time) value of major stresses in the MAR tectonogenesis zone; however, analysis of the reasons for these characteristics is beyond the scope of this work.

The following are important for analyzing the instability of multifault systems. The majority of events in the cross-correlation (Fig. 4) is focused in the shortest range of MAR segments (from 20 to 50 km) and they are more or less evenly distributed by range of lengths of the offset parts of transform fracture zones of 10—80 km. Taking into account that MAR segments with such a length form compact chains, especially in the equatorial Atlantic, this group could mainly represent multifault transform fracture systems where a short step of the MAR segment is combined with a longer step (by two three times) in displacement zones. Statistical characteristics indicate that these systems are a specific type of transform fracture zones, which is clearly individualized in the geometric plot. The St. Paul system is the most striking

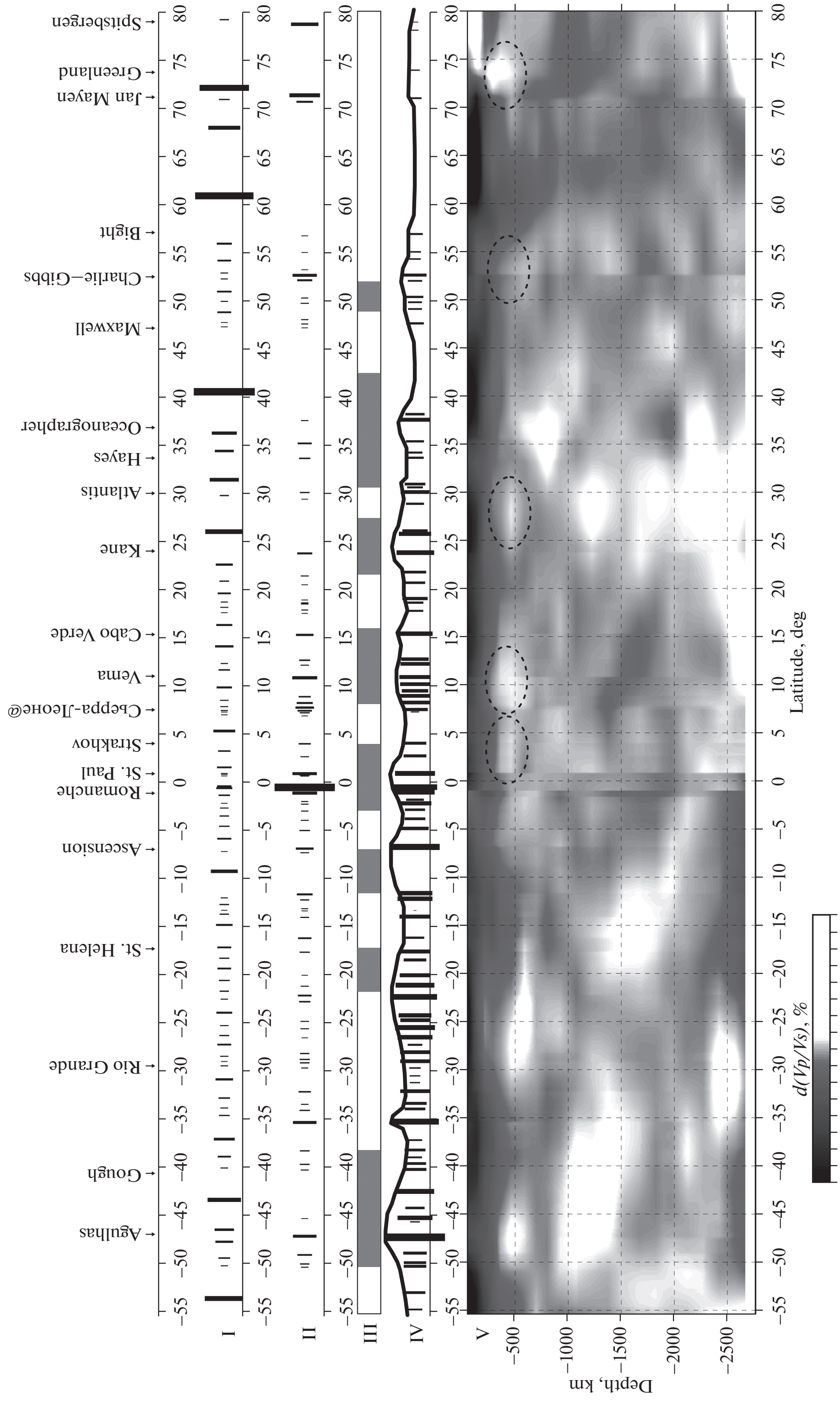

Fig. 5. Correlation of characteristics of MAR structural elements (I–IV) and cross section of variation in Vp/Vs (V) after [8]. I, center of MAR segments (symbol size is linearly proportional to segment length, from 18 to 1186 km) and titles of major fracture zones; II, position of offset zones of transform fracture zones (the symbol size is linearly proportional to offset length, from 10 to 750 km); III, position of zones with anomalous combination of reductions of gravity field [22]; IV, average position of transform fracture zones (symbol size is linearly proportional to total length with passive parts) and their envelopes [6]; V, variations in Vp/Vs (V) calculated by seismotomographic data for P and S waves [10, 15, 23]; dotted circles, cold anomalies of upper mantle in equatorial and northern Atlantic.

example of these (Fig. 1). Considering the hypothetical presence of spreading segments [1] with along-axis processes, which are spatially limited by the offset zones, we can suggest that, in case of multifault systems, spreading segments should be 25 km wide and ~150 km deep. This depth for partly melted mantle material is determined by the depth of the axial anomaly of variation in S waves, the estimate of which approaches 100–150 km with increasing precision of current seismotomographic models [17]. At a spreading segment size ratio of 1 : 6, convection is unstable [12]; thus, the presence of the typical independent three-dimensional convective-spreading process is unlikely in a cell 25 km in size and 150 km deep. Most likely, short MAR segments in multifault systems show the current position of the extension zone in a wide shear zone and could mismatch the position of the center of mantle upwelling.

COMPARISON OF MAR CHARACTERISTICS WITH THE SEISMOTOMOGRAPHIC SECTION

The characteristics of MAR structural elements with bathymetry-based fragmentation described above reflect the deep state of the upper mantle. Figure 5 shows the correlation of these characteristics and the cross section of variation in the velocity ratio Vp/Vs according to [8], which was calculated by seismotomographic models [10, 15, 23]. The dotted circles show the "cold" anomalies of the upper mantle in the equatorial and northern Atlantic, which coincide with the ranges of maximum latitudinal displacement of the MAR zone.

Comparison allows us to see that extended (>300) MAR segments (Fig. 5-I) coincide with "hot" seismotomographic anomalies (Fig. 5-V), which is evident from the position of the centers of long MAR segments. Many such segments are especially located at the interception of the MAR by the Iceland and Azores plumes and in the southern branch of the African superplume. The positions of displacement zones of transform fracture zones (Fig. 5-II) consequently divide the position of MAR segments, and their maximum concentration is observed in ranges that concentrate many short segments. In the equatorial and northern Atlantic, compact fault groups are located above the cold anomalies of the upper mantle in areas of maximum MAR latitudinal displacement. The couple of the Romanche Transform Fracture Zone, which is composed of two troughs meeting in the west, and the St. Paul multifault system is the most striking example of such a displacement. Above the cold upper mantle block, it includes the Arkhangel'skii–Doldrums–Vernadskii multifault system between 7 and 9 N and a group of the double system of the Marathon–Mercurius and Vema transform fracture zones north to 11 N. In the northern Atlantic, the MAR displacement above the cold anomaly passes along the doubled Charlie–Gibbs fracture system. North of the Iceland plume anomaly, there is also a combination of cold mantle and fracture zones with large displacement (Jan Mayen and Spitsbergen). Thus, a large displacement above the cold mantle could be expressed by usual transform displacements, but it is often split on doubled and multifault systems.

Figure 5-III shows the position of zones with an anomalous combination of a reduction in the gravitational field: the maximum value of the Bouguer anomaly and the minimum value of the isostatic anomaly, which are based on areal cluster analysis [6, 22]. Such a combination occurs, as a rule, in forearc zones, where broad thrust events form zones with increased deficit in masses and an increased Bouguer anomaly in the area of the lithosphere most remote from the spreading center. Probably, this is due to the presence of a significant longitudinal component of present-day movements, which results in the formation of latitudinal zones with activation of compression stresses [7] and corresponding deformations. Such a probability has been indicated by current GPS observations in adjacent continents [25]. Because we are discussing zones that correlate with fracture systems, longitudinal compression may lead to transpression along faults including their passive parts. The total lengths of the latter are shown in Fig. 5-IV according to [6] along with the curve of the envelope. It is evident that the concentration of transform fractures correlates with zones corresponding to the above combination of gravitational reductions. Coincidence of the densities of fracture zones (with passive parts) along the MAR with indirect features of longitudinal compression indicates the presence of an additional factor, which causes the characteristics of major MAR structural elements. The St. Paul multifault system, along with the Romanche transform fracture zone, is located within the equatorial "pulsation" of the parameters shown in Figs. 5-III and 5-IV.

SEISMICITY OF ACTIVE AREAS OF THE ST. PAUL MULTIFAULT SYSTEM

Analysis of the seismicity of active areas of the St. Paul system revealed the spatiotemporal and frequency-magnitude distribution of earthquakes. Data on seismic events with a magnitude of mb >3 are taken from the ANSS online catalog [26]. The data contain the dates of events up to tenths of a second, the coordinates, magnitude value, and index that indicates its calculation equation, the number of stations that registered the earthquake, the identification number of the event, the mean-square error, and the regional catalog (data source). In terms of accuracy in determination of coordinates, some earthquakes are inconsistent with the requirements of the study. The analyzed sampling includes events from 1979 to 2015 (Figs. 6a, 6b). This period spans 212 registered events that satisfy the analysis conditions. The range of magnitudes is 3.9–5.8 with a peak event with a magnitude of 4.7. Such a

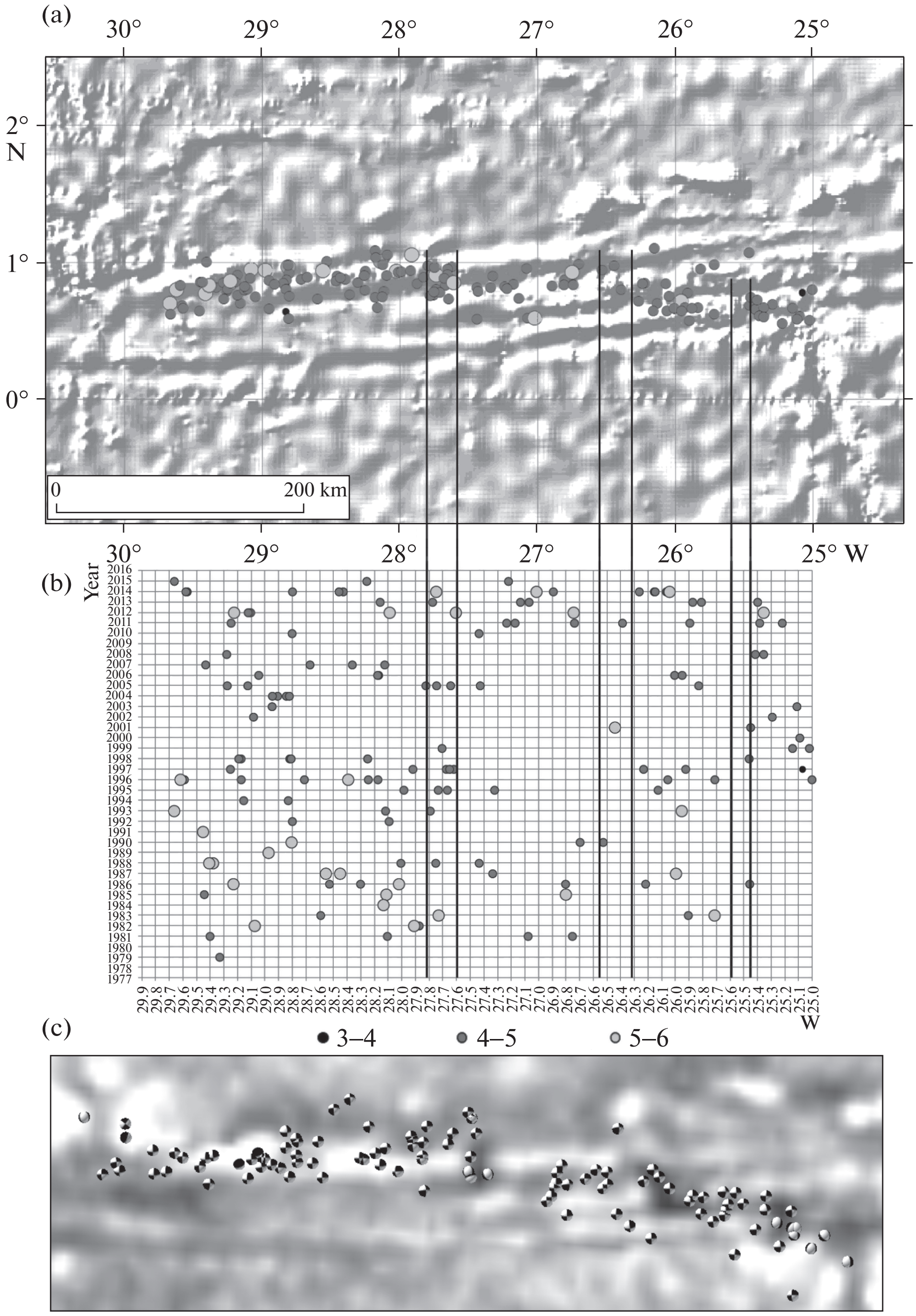

Fig. 6. Seismicity of St. Paul transform fracture system. A, epicenters of earthquakes on bathymetric map of region (magnitude of earthquakes is marked by size and gradation of gray circles) [26]; B, spatiotemporal distribution of seismicity in region (vertical lines mark position of rift segments); C, mechanisms of foci [27].

magnitude distribution of events is typical of MAR transform fracture systems with an increased amount of earthquakes with magnitudes of >5.

Within the reviewed territory, the MAR rift valley has been shifted many times by the St. Paul transform fracture system to the west (Fig. 6a). The spatial structure of earthquakes marks the active areas of fracture zones and MAR segments and makes it possible to decipher the current configuration of the spreading zone. The amplitude of displacements from south to north along the transform fracture zones increases to the west. The southern displacement has an amplitude of 36 km and is followed by a 20-km segment of the rift valley, the next segment is shifted 92 km and the rift valley is extended 28 km, a transform displacement 130 km long occurs to the west along with an area of the rift valley 28 km long, and the northernmost transform fracture zone is 200 km long. It is the most seis-

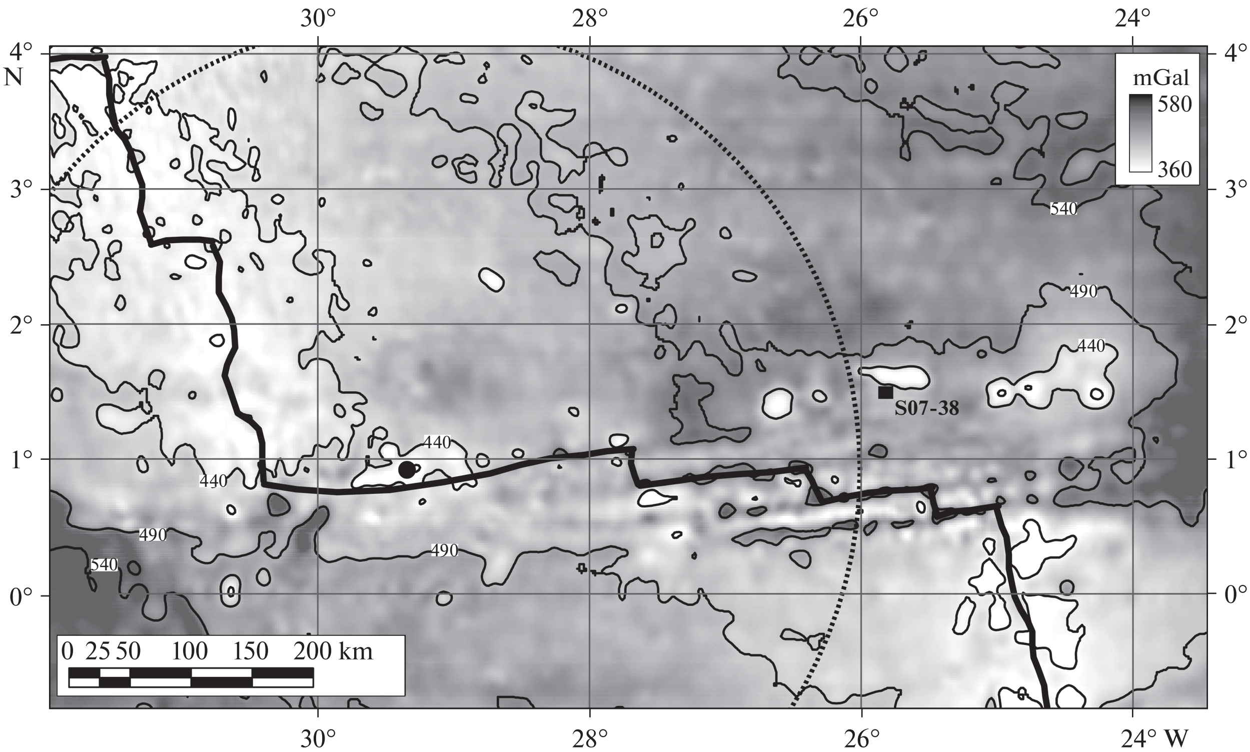

Fig. 7. Bouguer anomalies in St. Paul multifault transform fracture system and active MAR elements. range of values of anomalous field 360–580 mGal (from light to dark); major isodynams: 440, 490, and 540 mGal; dotted circle, 200-mile economic zone of Brazil around St. Peter and Paul islands.

mically active. The strongest events occur in the trough, whereas medium ones are focused in the southern wall of the fracture zone. The fracture zone with the 130-km shift, in contrast, is characterized by decreased seismic activity. Single events occur in the inactive sectors of transform fracture zones. The eastern and central parts of the rift valley are distinct in the decreased seismic activity in contrast to the western rift valley. According to geological data [18], precisely in this part of the fracture zone, active part of the fracture zone changes its position from the trough, which is located to the south of the St. Peter and Paul islands, to the trough to the north of it, which is the fifth in succession in the multifault system. The intensity of short-range seismicity of MAR segments is similar to that from the fracture zone. The data on the mechanisms of foci taken from the Harvard CMT catalog [27] are shown in Fig. 6c. No normal faults typical of the extension of rifts occur in the entire length of the St. Paul transform fracture system. Only three normal faults, two of which are oriented obliquely to the azimuth of the structure, are located in the western and eastern segments. The central segment has no features of foci with extensions. We have observed chains of oblique NW and NE displacement mechanisms along directions typical of Riedel shears, which cross cut more than one trough. This indicates the spatial mosaic character of stresses in the wide multifault system and the formation of oblique active zones wthathich cross cut major structural elements. Longitudinal thrusts are observed in the west, in the most active zone of transition from the fourth to the fifth troughs.

BOUGUER ANOMALIES AND VOLCANISM

In calculating Bouguer mantle anomalies (on the basis of usual Bouguer anomalies), the depth of the M boundary was estimated as the sum of the relief and thickness of the sedimentary cover and crystalline layer with a constant thickness of 6000 m. The difference in crust–mantle densities was 0.5 g/cm3. No thermal correction was done. The presence of an axial anomaly beneath the MAR, which indicates the existence of heated and partly melted mantle material leading to decompaction of the medium and the formation of minimums along this structure, is a major feature of this reduction in the gravitational field in the ocean. The Bouguer axial anomaly below the MAR to the south of the St. Paul system (Fig. 7) extends to the north up to a latitude of 1.50 N approximately along the 25 N meridian. Its end hosts a cluster of latitudinal symmetrical volcanic seamounts, which are manifested by local minimums in the Bouguer anomalies by an isodyname of 440 mGal and which indicates the probable formation of the couple of “bull’s eye” complexes from the local magmatic pulses. Such a continuation of the axial minimum to the abyss is rare. Similar volcanic complexes make up the main part of Researcher Ridge (south of the Vema transform fracture zone), but are shifted 250 km, on average, west of the MAR axis. Tracing of the fourth (from the south) fracture trough in the anomalous field up to the axis of the volcanic cluster reveals the possible position of the transform displacement zone. According to the ages of magnetic anomalies [19], the continuation of the MAR axis near the volcanic cluster may be ~25 Ma in age. Thus, the configuration of anomalous field shows the possible position of the MAR paleoaxis and indicates the spatial WNW displacement of active spreading elements. Basalts and breccias of volcanic glass collected from the bottom of this area (st. S07-38) at the southern foot of one volcanic edifice (Fig. 7) may indicate, in our opinion, off-axis magmatism.

SEISMIC PROFILING

The eastern part of the St. Paul system was studied by areal geophysical survey and continuous seismic profiling (CSP) on the seventh cruise of the R/V *Akademik Nikolai Strakhov* of the GIN RAS (Fig. 1) [13]. The survey area covered the most complex part of the system and the area of continuation of the gravitation minimum north of the MAR. The profiles in Figs. 8–11 show the important features of the wave field. Two profiles in the western (Figs. 8, 9) and eastern (Figs. 10, 11) parts were selected on a line of the MAR continuation.

The presence of "bright spot" anomalies at the foot of the cover is a feature of the profiles. The oceanic basaltic basement typically forms the wave field of the acoustic basement as a superposition of hyperbolas of distance from prominences of the basement. The profiles contain its reflectors, which are rather flat and characterized by increased reflection such that (Figs. 8, 9, 11) the amplitude in multiple reflections is comparable to bottom reflection from the sediment surface. A similar wave pattern corresponds to wide, quickly formed magmatic areas rather than to the ridgelike magmatic basement that formed during slow spreading. These could be eruptions of cover basalts (small traps) or effusive rocks, which lack the morphology of the acoustic basement relief typical of the MAR, whereas the flat volcanic surface forms coherent reflection with a large amplitude rather than the usual basement. The most intense reflections of this type are observed in the middle of the profile (Fig. 11), which is located almost in the north MAR continuation. The distance between the latitudinal volcanic range and bright spots of this profile is ~70 km. This is evidence that productive magmatic events are focused along seamount ranges (expressed by the minimums of Bouguer anomalies, Fig. 7) and south of them. The genesis of the source of productive magmatism in the MAR segment with a block of the cold upper mantle and the absence of plumelike seismotomographic anomalies is unclear, but this problem is beyond the scope of our work.

The gradual displacement of bright spots to the north from the first and second troughs (Fig. 11) to the third and fourth troughs (Fig. 9) and to the fourth and fifth troughs of the system (Fig. 8) is observed from the eastern (Fig. 11) to the western (Fig. 8) profile, as well as a regular increase in the thickness of sediments above the bright spots from 200 (Fig. 11) to 800 ms (Fig. 8). Spatiotemporally equal sedimentation rates indicate the spatial displacement of the magmatic source with time from north to south. However, because the presence of sedimentary "pockets" up to 800 ms thick only 100 km from the active zone of the MAR shows diverse and complex sedimentation conditions, we cannot guarantee southern displacement with time. All five troughs of the multifault system are visible in Figs. 9–11. They are currently active and host minimum sediments or are free of them. The northernmost walls of interfracture uplifts are more gently inclined and are questlike relief forms in cross section. A significant part of the sedimentary cover that fills the active and inactive troughs occurs horizontally and accumulated after the formation of major deformations (Figs. 9, 11), probably under transpression in a wide shear zone. This indicates that deformations are presedimentary. The sedimentary cover of the fifth trough in Fig. 9 is nonetheless deformed with the formation of an the incline as the axial bright spots (Fig. 11). These present-day deformations and a series of small faults in the third trough (Figs. 10, 11) are accompanied by acoustic brightening of the sedimentary thickness in the form of vertical bands 100 to 500 m wide. This indicates the contribution of fluids to sediments. The reason for this event may be either the current magmatism or serpentinization of ultramafic rocks due to their contact with water in the fracture zone. An example of a fluid vent on the surface is shown in Fig. 10 (inset map). It is located directly above the bright spot of the flattened basement with a vertical acoustically turbid zone, which is expressed on the surface as weak hyperbolas of dispersion and brightening of bottom reflections.

The wave field of this fluid vent differs from typical records with acoustic brightening; thus we believe that its origin is related to active magmatism. Typical vertical acoustic brightening in the second and third troughs (Figs. 9–11) is ascribed to the most widespread anomalies (discharge of gaseous serpentinization products) [3]. Thus, the seismic records show the presence of presedimentation magmatic zones, which form the anomalous acoustic basement beyond the currently active MAR segments, and presedimentation and present-day deformation stages of the oceanic crust.

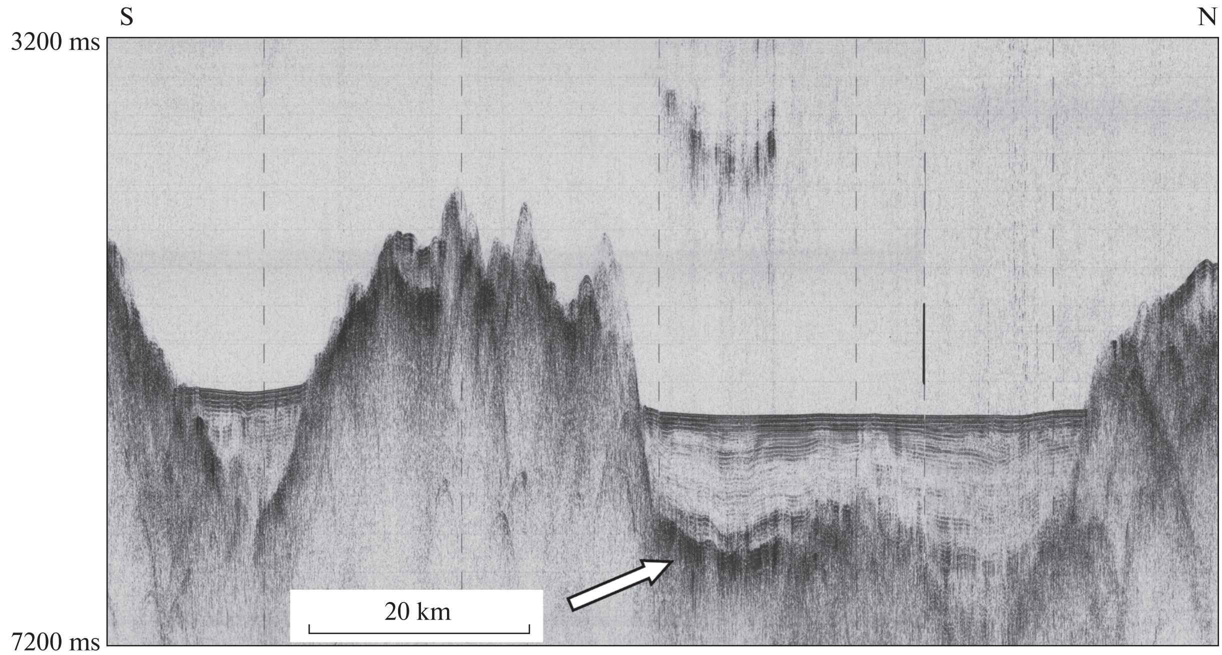

Fig. 8. Profile S07-SP-01a (seventh cruise of R/V *Akademik Nikolai Strakhov* (GIN RAS, 1988). Here and in Figs. 9-11, position of profile is shown in Fig. 1. Arrows, anomalies of bright spot record.

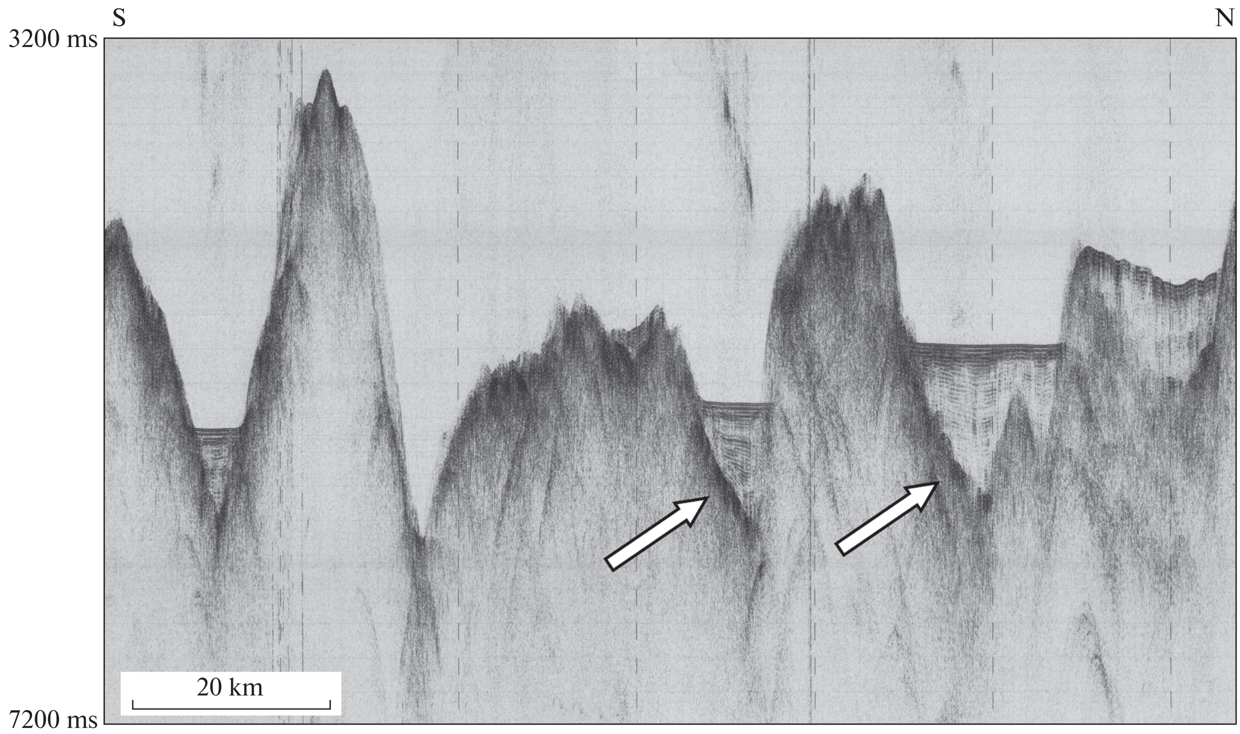

Fig. 9. Profile S07-SP-08.

STRUCTURE OF THE ACOUSTIC BASEMENT

CSP data of the seventh cruise of the R/V *Akademik Nikolai Strakhov* were used to draw a sediment thickness map on a scale of 1 : 650000 [5]. Subtraction of the digital model of the thickness of the sedimentary cover from the relief allowed us to obtain a map of the acoustic basement relief (Fig. 12). A depression up to 4900 m deep similar to nodal in terms of location and

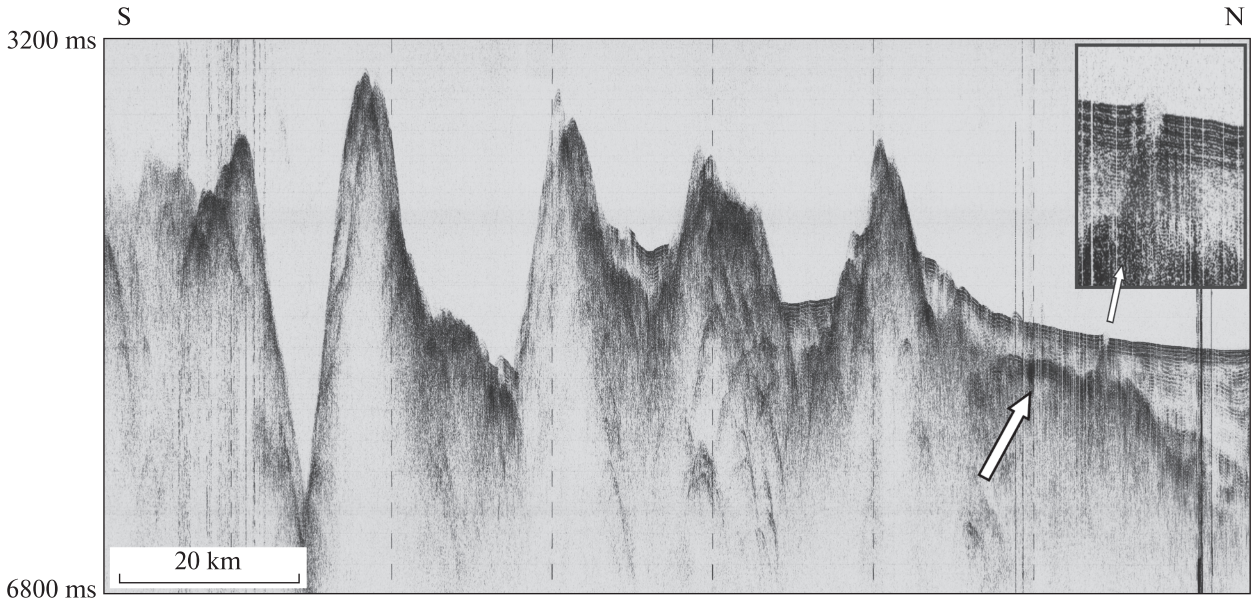

Fig. 10. Profile S07-SP-18. Inset, fragment of record with fluid vent above bright spot of basement.

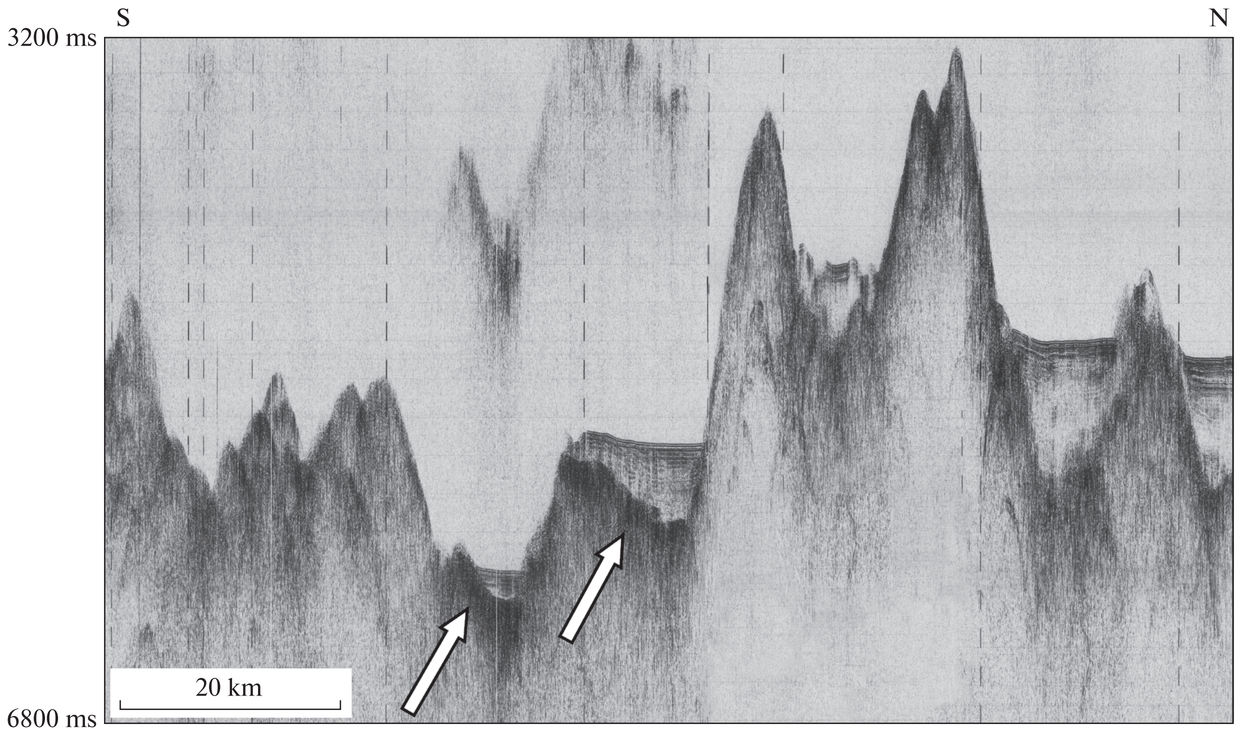

Fig. 11. Profile S07-SP-20.

morphology was found after subtraction of sediments with a maximum thickness up to 1100 m in the northeast part of the survey area between volcanic seamounts. The depression is located on the northern continuation of the MAR segment, which is characterized by the strongest bright spot (Fig. 11). The questlike relief of the interfracture ridges and small thickness (up to 250 m) of horizontal sediments indicate that the formation of the flattened magmatic basement and the segment's loss of activity were simultaneous with deformations, after which the sedimentary cover filled the depression of the basement in

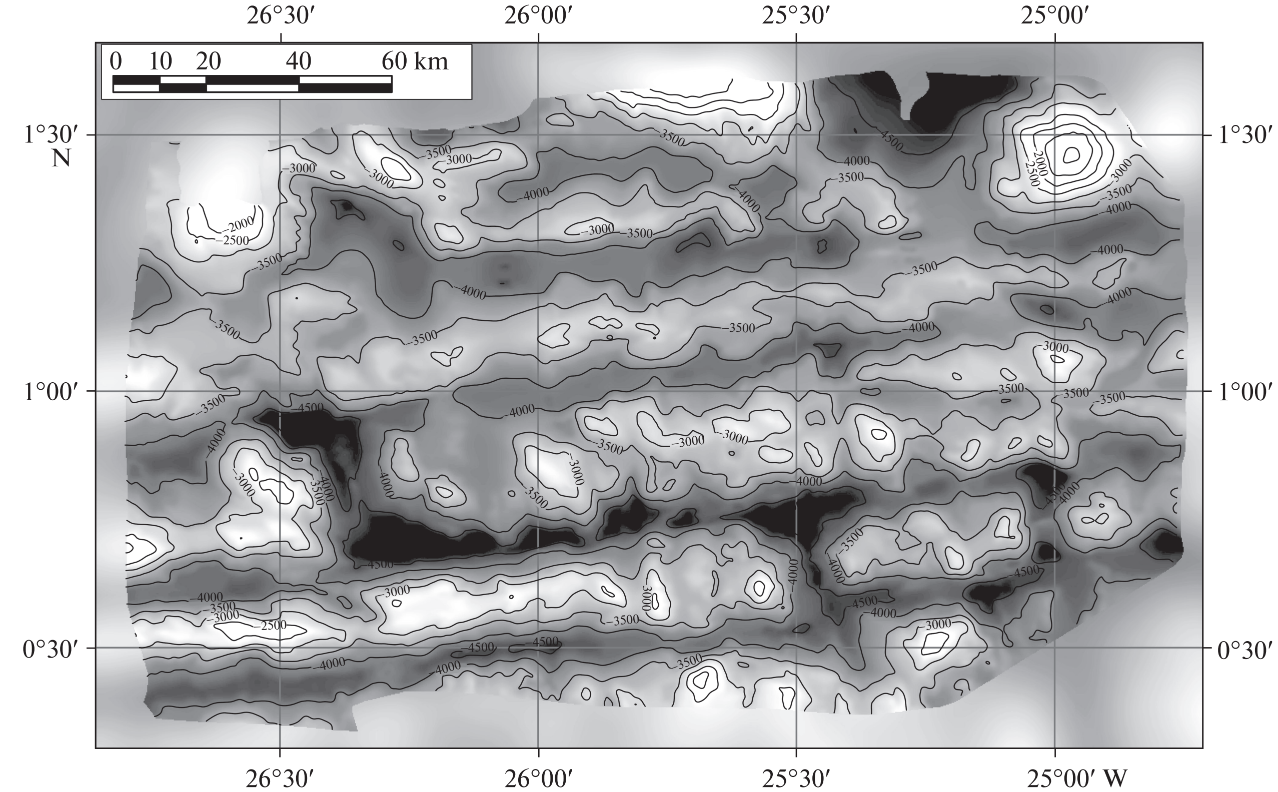

Fig. 12. Relief of acoustic basement in working area of seventh cruise of R/V *Akademik Nikolai Strakhov* (GIN RAS, 1988) in survey area of eastern part of St. Paul multifault transform fracture system. Relief ranges from –5370 to –700 m. Depth contours shown through 500 m.

the inactive segment. Probably, the change in the stress regime in the multifault system displaced the active segment to the west, to the weaker zone. The questlike forms of the basement occur in the latitudinal profile along the active part of the second trough with a flat eastern wall. This shows the complex character of deformations that form these structures on the longitudinal and latitudinal profiles. In addition to the paleonodal depression, the relief of the acoustic basement in the NW part of the survey area hosts a paleosegment of the rift valley between the fourth and fifth troughs, which was found after subtraction of sedimentary cover ~500 m thick. The distance between its paleonodal depression in the fourth trough and the present-day nodal depression of the fourth trough is 160 km, which indicates several possible jumps of MAR segments from east to west within bottom areas that are limited by lineaments of troughs of the multifault system. The MAR paleosegment is also observed in the southeast of the survey area, but the distance between it and the active segment of the first and second troughs is only ~50 km. Thus, the relief of the acoustic basement is evidence of jumping of active parts of the MAR. They could jump several times and, if the thickness of sediments is proportional to their age, the new active elements formed from north to south.

SYNTHESIS

The aforesaid data and results of their analysis allows the following summary. Figure 13 shows the map of the region of the St. Paul multifault system (five fracture troughs) with elements of geodynamic interpretations. The short rift segments jump along the strike of parallel troughs for distances that exceed the length of the segments. The troughs of the multifault system specify the limits of jumps within which the momentary position of segments is unstable and may change depending on the redistribution of stresses. Under transpression, the segments change their position to correspond more to the current stress pattern in a complex system consisting of small (20–40 km) blocks. In the equatorial Atlantic, MAR rift segments are shifted by the St. Paul multifault fracture zone system from north to south and to the west with increasing amplitude of displacement (Fig. 13). Contemporary earthquakes mark the active areas of fracture zones. According to [18], the active shear segment is now jumping from the fourth trough to the south of the St. Peter and Paul cliffs to the fifth trough north of

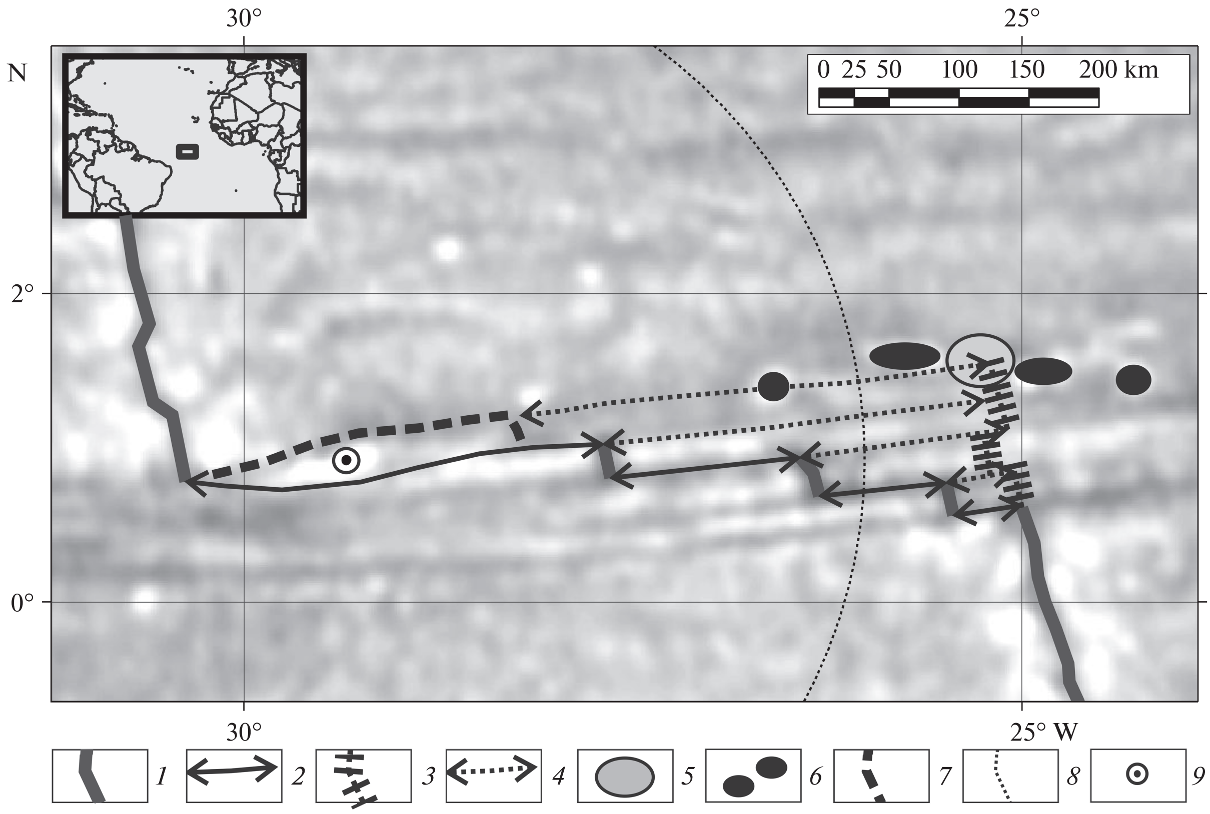

Fig. 13. Scheme of migration of active MAR segments in St. Paul multifault transform fracture system. (*1–3*) Segments of (1) active rift, (*2*) active transform fracture zone, (*3*) paleorift, (*4*) possible trajectory of rift jump, (*5*) paleonodal depression filled with sediments (>1100 m), (*6*) large volcanic edifices, (*7*) trajectory of present-day jump in active segments of transform fracture zone [18], (*8*) economic zone of Brazil, (*9*) St. Peter and Paul islands.

them, so these islands are moving from the African Plate to the South American Plate.

Thus, under longitudinal superposition of two spreading centers (from St. Paul in the west to the volcanic seamount in the east) for 120 km, the system of active spreading elements is reorganized so that the transition between their continuations is the shortest in the latitudinal direction. We have also observed straightening of the transition between large MAR segments by the fracture zone. A similar strike and step of multifault transform fracture systems are observed north of this region in the Arkhangel'skii–Doldrums–Vernadskii fracture systems and the double Marathon–Mercurius system; they are caused by macroscopic plate kinematics.

CONCLUSIONS

1. Cross-correlation of the lengths of active MAR structural elements (ridge segments and transform fracture zones of displacement) shows that major events are focused in the shortest MAR segments from 20 to 55 km and are evenly distributed over the lengths of active parts of fracture zones of 10–80 km. MAR segments with these parameters in the equatorial Atlantic form compact chains, which are multifault transform fracture systems. Here, a short step along a MAR segment is combined with a longer (by two to three times) step in the displacement zones and this combination is periodically repeated. Statistics indicate that these systems represent a specific type of transform fracture zones.

2. Multifault and doubled transform fracture systems occur between segments where the MAR axis is displaced the most in latitude and the upper mantle contains cold blocks according to the seismotomographical data. The increased density of the total lengths of fracture zones including passive parts is also related to these fracture systems and the presence of zones with longitudinal compression, which leads to transpression along the faults, is determined indirectly.

3. Seismicity distinguishes currently active segments of the spreading system with increasing amplitudes of displacement from east to west along fracture troughs. Almost the entire zone contains no events with normal faults and represents linear groups of displacements, which are often obliquely oriented to major chain elements.

4. The axial Bouguer anomalies of the MAR continue for 120 km to the north from the active segments

of the St. Paul zone and end by the latitudinal zone of the volcanic edifices.

5. Seismic profiling shows the presence of anomalous bright spot reflectors, which correspond to flattened magmatic basement that originated during productive magmatism different from that of slow spreading zones. These reflectors are overlapped by horizontal sedimentary cover with decreased thickness to the south. Deformations of the acoustic basement are mainly presedimentation. Present-day deformations with lower amplitude in comparison with the basement are accompanied by vertical acoustic brightening of the sedimentary cover. There are features of contribution of fluids to the water column.

6. The structure of the acoustic basement hosts segments of rift paleovalleys and a paleonodal depression, which mismatch the position of the currently active zones. The location of the paleoform indicates several jumps in the rift and, correspondingly, displacement segments.

7. The multifault transform fracture system with five trough (in addition to the displacement component of movement), which is affected by longitudinal tension probably variable in time and direction, is unstable in the position of the rift segments inside it, which could jump in its limits according to the redistribution of stresses and the formation of more optimal rifting conditions in another location. Straightening of the transform transition between two remote MAR segments is observed in the St. Paul multifault system.

ACKNOWLEDGMENTS

The authors thank the crew of the R/V *Akademik Nikolai Strakhov* for selfless work under trying conditions as we obtained material for this paper. This work was conducted in the under State Contract no. 01201459183 "Estimation of Relation of the Bottom Relief of the Atlantic Ocean and the West of the Arctic Ocean, Deformations of the Sedimentary Cover, Degassing Processes, and Dangerous Geological Events with the Geodynamic State of the Crust and Upper Mantle." This work was also supported by the Russian Foundation for Basic Research (project nos. 15-05-05888, 13-05-12076-ofi_m, 14-05-00122), the Presidium of the Russian Academy of Sciences (program nos. I.18P, I.43.P, II.3P), and a Presidential Grant in Support of Leading Scientific Schools (project no. NSh_5177.2012.5).

REFERENCES

1. S. V. Aplonov and A. A. Trunin, "Migration of spreading local instability along the axis of divergent boundary: The Mid-Atlantic Ridge between the Marathon and Kane transform faults," Fiz. Zemli, No. **9**, 24–34 (1995).
2. L. V. Dmitriev, S. Yu. Sokolov, V. G. Melson, and T. O'Hirn, "The plume and spreading associations of basalt and their reflection in the petrological and geophysical parameters of the northern Mid-Atlantic Ridge," Ross. Zh. Nauk Zemle **1**, 457–476 (1999). doi 10.2205/1999ES000025
3. L. V. Dmitriev, B. A. Bazylev, S. A. Silantiev, M. V. Borisov, S. Yu. Sokolov, and A. Bugo, "Hydrogen and methane formation with serpentization of mantle hyperbasite of the ocean and oil generation," Ross. Zh. Nauk Zemle **1**, 511–519 (1999). doi 10.2205/2000ES000030
4. A. O. Mazarovich, *Geologic Structure of the Central Atlantic: Faults, Volcanic Edifices, and Ocean Floor Deformations* (Nauchnyi Mir, Moscow, 2000) [in Russian].
5. A. O. Mazarovich, S. Yu. Sokolov, G. V. Agapova, K. O. Dobrolyubova, V. N. Efimov, "Computer technologies used to obtain new information on crustal structure in oceanic fracture zones: A case study on the active segment of Sao Paulo Fracture Zone, Central Atlantic," Russ. J. Earth Sci. **3**, 59–78 (2001). doi 10.2205/2001ES000055
6. N. S. Sokolov, "Correlation of the geological and geophysical parameters along the axis of the Mid-Atlantic Ridge and pre-arc settings on its eastern flank," Moscow Univ. Geol. Bull. **62**, 404–409 (2007).
7. S. Yu. Sokolov, "Anomalous focal mechanisms of earthquakes in the Atlantic and their geodynamical interpretation," in *Geologiya morei i okeanov: Materialy XVIII Mezhdunarodnoi nauchnoi konferentsii (shkoly) po morskoi geologii* (GEOS, Moscow, 2009), Vol. 5, pp. 153–155.
8. S. Yu. Sokolov, "The state of geodynamical mobility in the the mantle from seismic tomography and ratios between velocities of *P*- and *S*- waves," Vestn. KRAUNTs. Nauki Zemle, No. **2**, 55–67 (2014).
9. A. V. Tevelev, *Shear Tectonics* (Mosk. Gos. Univ., Moscow, 2005) [in Russian].
10. T. W. Becker and L. Boschi, "A comparison of tomographic and geodynamic mantle models," Geochem., Geophys., Geosyst. **3**, Pap. No. 2001GC000168 (2002). doi 10.1029/2001GC00016810.1029/2001GC000168
11. D. Brunelli and M. Seyler, "Asthenospheric percolation of alkaline melts beneath the St. Paul region (Central Atlantic Ocean)," Earth Planet. Sci. Lett. **289**, 393–405 (2010).
12. S. Chandrasekhar, *Hydrodynamic and Hydromagnetic Stability* (Clarendon, Oxford, 1961).
13. *Equatorial Segment of the Mid-Atlantic Ridge. Initial Results of the Geological and Geophysical Investigations under the EQUARIDGE Program, Cruises of R/V "Akademik Nikolaj Strakhov" in 1987, 1990, 1991*, Vol. 46 of *Intergovernmental Oceanographic Commission, Technical Series* (UNESCO, 1996).
14. D. J. Fornari, D. G. Gallo, M. H. Edwards, J. A. Madsen, M. R. Perfit, A. N. Shor, "Structure and topography of the Siqueiros Transform Fault System: Evidence for the development of intra-transform spreading centers," Mar. Geophys. Res. **11**, 263–299 (1989).
15. S. P. Grand, R. D. Van der Hilst, and S. Widiyantoro, "Global seismic tomography: A snapshot of convection in the Earth," GSA Today **7** (4), 1–7 (1997).

16. M. Ligi, E. Bonatti, L. Gasperini, and A. N. B. Poliakov, "Oceanic broad multifault transform plate boundaries," Geology **30**, 11–14 (2002).

17. S. Lebedev and R. D. Van der Hilst, "Global upper-mantle tomography with the automated multi-mode surface and *S* waveforms," Geophys. J. Int. **173**, 505–518 (2008). doi 10.1111/j.1365-246X.2008.03721.x

18. K. F. Motoki, A. Motoki, and S. E. Sichel, "Gravimetric structure for the abyssal mantle massif of Saint Peter and Saint Paul peridotite ridge, Equatorial Atlantic Ocean, and its relation to active uplift," An. Acad. Bras. Cienc. **86**, 571–588 (2014).

19. R. D. Müller, M. Sdrolias, C. Gaina, and W. R. Roest, "Age spreading rates and spreading asymmetry of the world's ocean crust," Geochem., Geophys., Geosyst. **9** (4), Pap. No. Q04006 (2008). doi 10.1029/2007GC00174310.1029/2007GC001743

20. D. T. Sandwell and W. H. F. Smith, "Global marine gravity from retracked Geosat and ERS-1 altimetry: Ridge segmentation versus spreading rate," J. Geophys. Res.: Solid Earth **114**, Pap. No. B01411 (2009). doi 10.1029/2008JB00600810.1029/2008JB006008

21. J. G. Sclater, N. R. Grindlay, J. A. Madsen, and C. Rommevaux-Jestin, "Tectonic interpretation of the Andrew Bain transform fault: Southwest Indian Ocean," Geochem., Geophys., Geosyst. **6** (9), Pap. No. Q09**K10** (2005). doi 10.1029/2005GC000951

22. S. Yu. Sokolov, N. S. Sokolov, and L. V. Dmitriev, "Geodynamic zonation of the Atlantic Ocean lithosphere: application of cluster analysis procedure and zoning inferred from geophysical data," Russ. J. Earth Sci. **10** (4), Pap. No. ES4001 (2008). doi 10.2205/2007ES00021810.2205/2007ES000218

23. R. D. Van der Hilst, S. Widiyantoro, and E. R. Engdahl, "Evidence of deep mantle circulation from global tomography," Nature **386**, 578–584 (1997).

24. J. I. Wendt, M. Regelous, Niu Yaoling, R. Hekinian, and K. D. Collerson, "Geochemistry of lavas from the Garrett Transform Fault: Insights into mantle heterogeneity beneath the eastern Pacific," Earth Planet. Sci. Lett. **173**, 271–284 (1999).

25. Jet Propulsion Laboratory, California Institute of Technology, 2014. http://sideshow.jpl.nasa.gov/post/series.html

26. Advanced National Seismic System (ANSS), USA, 2015. http://www.ncedc.org/anss/catalog-search.html

27. Harvard Centroid Moment Tensor (CMT), USA, 2013. http://www.globalcmt.org/CMTsearch.html

Translated by I. Melekestseva

SPELL: OK